

**NANO-PARTICLE REINFORCED POLYMER FOR BLAST PROTECTION OF
UNREINFORCED MASONRY WALL:
LABORATORY BLAST LOAD SIMULATION AND DESIGN MODELS**

M. IRSHIDAT, A. AL-OSTAZ, A.H.-D. CHENG, AND C. MULLEN

Nano Infrastructure Research Group-Department of Civil Engineering
University of Mississippi
Oxford, Mississippi, 38677-1848, USA

ABSTRACT

This paper investigates the performance of a new generation of nano-particle reinforced polymeric materials, as an alternative to fiber reinforced polymer (FRP), for the protection of masonry structures against blast loads. The nano-particles used in this study include the exfoliated graphene nano platelets (XGnP), and the polyhedral oligomeric silsesquioxane (POSS). The polymer is polyurea. One quarter scale physical model of unreinforced masonry walls, spray coated with the nano-particle reinforced polymers, are subjected to blast load in the ERDC Blast Load Simulator facility. It is observed that POSS reinforced polyurea significantly enhanced the performance of masonry walls sustaining blast load; while XGnP reinforcement has only marginal improvement. To build a numerical simulation and engineering design capability, computer model using ANSYS AUTODYN and simplified analytical model are constructed. These models predict fairly well the observed laboratory tests.

1. INTRODUCTION

The emergence of nanotechnology during the last decade has drastically altered the landscape of science and engineering. Nano-particle reinforced materials have superior mechanical, thermal, electrical, magnetic, and electromagnetic properties, which can be utilized for a new generation of infrastructure materials. By creating nanometer-scale structures, it is possible to control the physical properties of materials (strength, hardness, toughness, melting temperature, etc.) without changing the chemical composition. While several investigations are currently underway to characterize the macroscopic static properties of nano-particle reinforcements, there are few reported studies on the effects of using such materials in dynamic response concerning blast/shock/impact loadings. Another critical issue for the development of nanotechnology is the ability to understand, model, and simulate the behavior of its small structures and to make the connection between these properties and their macroscopic functions.

One of the greatest threats from blast loading is the fragmentation pieces from walls, windows, equipment, or vehicles flying at high speeds that they can result in extensive injury or death. Un-reinforced masonry (URM) walls have low resistance to out-of-plane loadings, particularly air blast load, due to low flexural capacity and tendency of brittle mode failure. These problems lead to a critical need to develop effective retrofitting techniques to improve the load carrying capacity of such members to resist blast loads. Many studies have been conducted on using retrofitting techniques to improve blast resistance capacity of concrete masonry unit (CMU) walls, including:

- Adding mass to the wall system by increasing thickness with a back-up wall comprised of masonry, concrete, or some type of steel framing system.

- Adding vertical steel members as a back-up system to greatly reduce the span requirements of the masonry wall system.
- Using Fiber Reinforced Polymer (FRP) composites adhered to the surface of the wall to better resist high flexural stresses.

The first two approaches (Myers et. al. 2004) involve significant disruption to structure occupants in terms of installation time and loss of usable floor space. Alternatively, Myers et al. (2004) experimentally investigated the efficiency of using FRP for the protection of existing and new masonry buildings against blast loads as an alternative to traditional concrete or steel retrofit. They concluded that FRP composites offer great benefits for strengthening masonry walls' resistance to blast loads. The composites have also been proven to remarkably increase the out-of-plane flexure capacity of URM elements' resistance to various blast threat levels, but the retrofitting has to be associated with proper shear capacity and wall-to-frame connections. Davidson, et al (2004) used full-scale explosive tests to determine the effectiveness of using sprayed-on polymers to improve blast resistance of unreinforced masonry walls. They concluded that a sprayed-on polymer retrofit approach to strengthening masonry walls against blast loads was an effective technique. Johnson, et al (2005) conducted a series of static and dynamic experiments to investigate the potential benefits of using both reinforced and unreinforced elastomeric materials to retrofit hollow, unreinforced, concrete masonry walls. The static experimental results demonstrated an increase in the ultimate flexural resistance of the retrofitted CMU walls. And it supported the idea that the polyurea spray-on materials did significantly increase the stiffness of the reinforced polyureas as compared to the unreinforced ones. Dynamic results showed that the unreinforced polyureas did add minor additional flexural resistance to the hollow unreinforced CMU wall, whereas the addition of reinforcement to the polyurea retrofit

system significantly increased the flexural resistance of the CMU walls. This increase in flexural resistance was directly related to the strength of the reinforcement, and as how the orientation of the fibers. The full-scale dynamic test results demonstrated the ability of the retrofit systems to mitigate the hazards associated with hollow unreinforced CMU walls. Davidson, et al (2005) experimentally and numerically studied damage and failure mechanisms of polymer reinforced concrete masonry walls subjected to blast loadings. They observed that a thin elastomeric coating on the interior face of the wall can be effective in minimizing the fragmentation and potential for collapse of unreinforced concrete masonry walls resulting from a blast. They also found that the elongation capacity was more important for damage reduction than having a high stiffness, so an effective balance between stiffness and elongation potential was required. Finite element results indicated that a spray-on polymer reinforcement approach can be effective in reducing the vulnerability of unreinforced CMU walls subjected to blast loading. Muszynski and Purcell (2003) discussed using of composite reinforcement to strengthen concrete and air-entrained concrete masonry walls against air blast. They concluded that retrofitting existing structures with high-strength composite materials provided an inexpensive method for structural hardening against the effects of air blast from a conventional weapon. Ghobarah and El-Mandooh (2004) investigated effective and practical approaches for strengthening URM block walls with openings for resistance to extreme out-of-plane loads. They concluded that the lateral load carrying capacity of the strengthened walls was significantly higher than that of the unstrengthened walls yielding a much more ductile performance.

Evaluating blast resistance of CMUs was the focus of many numerical investigations. For example, Eamon, et al. (2004) analyzed CMUs subjected to blast pressure using the Finite Element Method. Their model had the ability to replicate experimental results with good

agreement, generally matching the failure shape, the location of break lines, and the size and the number of primary pieces of debris.

An analytical approach was also one of the techniques used to evaluate the behavior of CMUs during blast loads. Single Degree of Freedom (SDOF) model and Iso-Damage curves were most often used for this purpose. For example, Naito and Wheaton (2006) presented a methodology for assessing the performance of structural elements subjected to explosive loading. This method combined Basic Section Analyses, equivalent SDOF modeling, and a Static Finite Element Pushover Analysis to calculate the blast resistance of an existing shear wall subjected to an external explosion. Their analysis revealed that the dynamic models allowed for the development of Pressure-Impulse resistance curves for the wall system. The available *P-I* resistance indicates that the walls were capable of resisting elevated dynamic blast pressures before collapse. Myers, et al (2004) developed an analytical model to predict the dynamic response of the URM walls strengthened with FRP using a simplified SDOF analysis approach.

It is clear from this abbreviated introduction that studies regarding nano particle reinforced polymers to protect structures against blast or sever loading conditions were limited, making it necessary to better understand the behavior of these materials and to take advantages of their superior properties. The main objective of this paper is to investigate the viability of using nano particle reinforced composites to protect masonry structures against blast loads experimentally, numerically, and analytically. Nanoplatelet reinforced polymers using exfoliated graphene nano platelets (XGnP) and Polyhedral Oligomeric Silsesquioxane (POSS) were used in this research to protect masonry walls against blast loads. The polymer used was polyurea Line-XS 350 produced by Protective Coatings Inc. Nanoplatelet reinforced polymers were used because they were low cost, high performance structural materials.

2. MATERIAL CHARACTERIZATION

Characterization of material properties is essential to identify those materials that are best suited for use in blast protection applications, to understand the panel response to blast loads, and to develop accurate predictive models that will form the basis of future design criteria. In this paper, mechanical properties of nano particle reinforced composites are evaluated for use as structural retrofits for panels subjected to air-blasts.

a. Quasi static test

A Uni-Axial Direct Tensile Test was performed using Material Testing and Simulation (MTS) machine (Figure 1) to identify the mechanical properties of materials used in this research. As mentioned previously, nanoplatelet reinforced polymers using exfoliated graphene nano platelets (xGnP) from XG-Sciences and Polyhedral Oligomeric Silsesquioxane (POSS) from Hybrid Plastics Incorporation were used to protect masonry walls against blast loads. The polymer used in was polyurea Line-XS 350 produced by Protective Coatings Inc. Six coupons were tested for each material: unreinforced polyurea; Exfoliated Graphene Nano Particle (xGnP) reinforced polyurea; and Polyhedral Oligomeric Silsesquioxane (POSS) reinforced polyurea, and the results averaged.

Determining the tensile stress-strain response for these materials was the main gain of this testing. Modulus of elasticity, tensile strength, and strain at failure were obtained from the stress-strain curves for each material. Typical stress-strain curves and typical mechanical properties of these materials are shown in Figure 2 and Table 1 respectively. Adding POSS particles to reinforce polyurea did not affect either the strength or the stiffness of the unreinforced polyurea under quasi-static condition; however, adding xGnP particles clearly decreased both the strength and the stiffness of the unreinforced polyurea

3. EXPERIMENTAL PROGRAM

Quarter scale model walls made of scaled down brick units (Figure 3) were used to investigate the response of retrofitted CMUs to external blast loads. The average mass of the brick units was 252 gm. The walls were fully grouted using approximately 16 blocks for height and 12 blocks for width as shown in Figure 3. The wall was cast in a steel frame with dowels set at top and bottom to simulate simply supported conditions and free boundary conditions at left and right. The average unconfined compressive strength and the density of the mortar were 15.9 MPa and 1.700 kg/m³, respectively, and the average unconfined compressive strength and density of the grout were 15.9 MPa and 1.800 kg/m³ respectively.

a. Test matrix

Three CMU walls were tested at the US Army Engineer Research and Development Center (ERDC) using the blast simulator (Figure 4). These were: retrofitted with unreinforced polyurea and retrofitted with reinforced polyurea using XGnP and POSS respectively.

Test matrix of retrofit schemes is summarized in Table 2. The polyurea used in was LINE-X XS-350 produced by Protective Coatings Inc.; POSS was provided by Hybrid Plastic Inc.; and XGnP was manufactured by XG-Sciences.

b. Experimental setup

A spraying technique was used to apply polyurea or nano-reinforced polyurea to the back (interior face) of the CMU walls (Figure 5). This technique was used because of the fast reaction between the polyurea resin and the *cyanates* hardener. The walls were sprayed going back and forth three times. Various retrofitted layer thicknesses were observed for each wall, Table 3, due to the difference in the viscosity of the materials and application process.

A pre-adjusted air blast pressure and impulse were applied to each wall. Nine pressure sensors

mounted on the steel loading frame were used to collect pressure time history (Figure 6). Typical pressure time history and calculated impulse time history were shown in Figure 7. For all cases there was an initial rise to a peak reflected pressure (compression pressure wave), followed by a decay to zero pressure, and then a negative phase (suction pressure wave). Therefore, if a wall system can be retrofitted adequately to resist the initial compression pressure wave, it can be allowed to fail on the opposite side (non occupant side) when subjected to the negative pressure wave. Average values of the reflected pressure and impulse subjected to each wall were summarized in Table 4.

c. Experimental investigations

Wall #1

At the end of the experiment wall #1 experienced horizontal crack at every horizontal mortar line throughout the blast events until it suffered a tensile failure at its horizontal mid-height mortar joint at blast peak pressure of 208.22 kPa (30.20 psi) resulting in collapsing of the wall (Figure 8). However, the retrofit helped the debris to remain intact and prevented it from entering the test structure.

Wall #2

Wall #2 sustained a significant damage. Every horizontal mortar line cracked. The primary damage was a horizontal crack that formed over the entire width of the wall at blast peak pressure of 224.91 kPa (32.62 psi) (Figure 9). However, the retrofit helped the debris to remain intact and prevented it from entering the test structure.

Observations of the previous two cases revealed that a thin elastomeric coating on the interior face of the CMU walls was effective at minimizing the fragmentation resulting from blast.

Wall #3

Wall #3 had hairline shear and horizontal crack at blast peak pressure of 218.91 kPa (31.75 psi). Shear damage was observed at the top left corner of the wall at the same peak pressure. The results showed that the addition of POSS reinforcement to the polyurea retrofit system increased the flexural resistance of the CMU wall significantly. The retrofit prevented the whole panel from being damaged (Figure 10).

An accelerometer and a laser sensor were used to measure mid-point deflection for each wall. The results are summarized later.

4. COMPUTATIONAL MODELING USING FINITE ELEMENT METHOD

To study the effect of blast loads on CMU walls and to understand the behavior of these structures under previously noted loading conditions, a number of experiments is required to get enough data that allow the researchers to analyze clearly and process the results. Unfortunately, the expense involved in blast experiments limits the number of tests that are predictable at a given time. Alternative methods as substitutes for actual experimentation had to be sought. The focus of this part of the paper was to develop a computationally-efficient model that can replicate with reasonable accuracy the wall failure mechanisms and midpoint deflection retrofitted CMU walls subjected to blast loads. Finite Element (FE) models provide cost and time effective solutions compared to the experimental alternative. A finite Element model was built into this research to predict the experiments as mentioned previously in this research. Due to time and cost constraints of the research program, development of a specific finite element analysis code for this project was not feasible. Therefore, ANSYS AUTODYN, an explicit hydrocode that used finite difference, finite volume, and finite element techniques to solve a wide variety of non-linear dynamic problems in solids, fluids, gases, and their interactions, was used to model and

analyze the Nano Reinforced Elastomeric Materials retrofitted masonry walls subjected to blast loading.

a. FE Model Configurations and Mesh

The importance of the computational modeling was measured by the ability of the finite element model to replicate with reasonable accuracy the experimental behavior of the system. Therefore, the same 16 blocks tall and 12 blocks wide CMU walls used in the experimental work were modeled using finite element software called AUTODYN. Each retrofitted CMU wall was represented by 8670 Lagrangian cells, 3840 of which were filled with masonry material to represent the bricks; 2440 were filled with the mortar material bonding the bricks together; with remainder represented the retrofitted material. Figure 11 shows the geometry and the mesh of the CMU walls.

b. Loading condition

As mentioned before, the focus of the FE work was to develop a computationally-efficient model that can replicate the wall failure mechanisms of retrofitted CMU walls subjected to blast loads. The model must employ the pressure-time history extracted from the shock tube blast simulator (Figure 7) as applied to a uniformly distributed load on the front side (un-retrofitted face) of the CMU wall.

c. Material Modeling

To model any material in AUTODYN, the parameters of equation of state (EOS), strength model, and failure model should already be defined.

Unreinforced masonry

The response of masonry under shock loading was a complex phenomenon. In this paper, a variety of constitutive models for the dynamic and static response of masonry have been

proposed over the years. Porous equation of state (EOS), Drucker-Prager strength model, and Hydrodynamic tensile failure (P_{\min}) model were used to represent the unreinforced masonry.

Mortar

Compaction equation of state (EOS), Mo Granular strength model, and Hydrodynamic tensile failure (P_{\min}) model were used to represent the mortar.

Retrofit materials

A real EOS should be defined for these new retrofitted materials; however, due to the low pressure level introduced by blast waves, a linear equation of state works as a start for this study. Equation 1 shows the linear EOS used to model all three retrofitted materials,

$$P = K\mu \quad (1)$$

Whereas, K was the material bulk modulus; μ was volumetric strain as given by Equation 2; ρ was the material density; and ρ_o was the reference density.

$$\mu = \frac{\rho}{\rho_o} - 1 \quad (2)$$

Elastic strength model and principal strain failure criterion were used to model these materials. All material models used in this research are summarized in Table 5. More details are available in AUTODYN Theory Manual.

5. RESULTS AND DISCUSSION

Wall #1

Results of FEA showed a maximum midpoint deflection of 102.61mm and maximum debris velocity of 4.44 m/s as compared to a maximum midpoint deflection of 91.4 mm and a maximum debris velocity of 3.86m/s obtained experimentally (Table 9). The wall failed at the middle; however, all debris was captured by the retrofit material. Unexpectedly, finite element results

showed a little (minor) damage for this case. Table 6 shows a comparison between experimental and numerical deformation shapes at time of maximum deflection and at the end of the test.

Wall #2

Results of FEA showed a maximum midpoint deflection of 113mm and maximum debris velocity of 6.14 m/s as compared to a maximum midpoint deflection of 76.4 mm and a maximum debris velocity of 7.47m/s obtained experimentally (Table 9). FEA experiments likewise showed that the wall failed in four main segments, and that all debris was captured by the retrofit material. Table 7 shows good agreement between experimental and numerical deformation shapes at the time of maximum deflection and at the end of the test.

Wall #3

Results of FEA showed a maximum midpoint deflection of 112 mm as compared to a maximum midpoint deflection of 95.65 mm obtained experimentally (Table 9). The wall did not fail in either experiment or FEA. Therefore, this was the most successful retrofit material. Table 8 shows good agreement between experimental and numerical deformation shapes at time of maximum deflection and at the end of the test.

The difference between the experimental and the computational results for wall #1 encompassed many possible explanations. First of all, as mentioned earlier in this paper, uniaxial tensile test was done using an MTS machine under a quasi-static condition to obtain the mechanical properties of the retrofit materials. These properties were fed into the finite element code to model the retrofitted walls under blast loads. It was clear from Figure 2 that both the polyurea alone and the polyurea reinforced with POSS had almost close to same stress-strain curve under quasi- static conditions, which meant that it should have same behavior during the test. This expectation was obtained from finite element analysis where the quasi-static properties

were used to model the retrofit materials. Experimentally, the wall retrofitted with polyurea alone failed (Table 6) while the wall retrofitted with POSS reinforced polyurea did not fail (Table 8). That meant that these kinds of materials had different behaviors and different properties under different strain rate conditions (strain-rate dependent). The retrofit layer thicknesses were not uniform over the whole wall. That may make some weak areas which can cause the experimental failure; whereas, in finite element model, a uniform thickness was applied over the entire wall.

6. SINGLE DEGREE OF FREEDOM (SDOF) SYSTEM

An SDOF system is one in which a single type of motion was possible. A typical SDOF system is the mass-spring-damper system shown in Figure 12 where the mass can move in a vertical direction only. In this system, the spring and damper are considered to have no mass and it is also assumed that the spring is linear. The force of gravity is omitted in this figure because the displacement of the mass (y) is measured from its neutral position, which the mass assumes in a static case where no load is applied. The equation of motion of the SDOF damped system subjected to an applied force $P(t)$ is:

$$m\ddot{y} + c\dot{y} + ky = P(t) \quad (3)$$

with m , c and k being system mass, damping coefficient and system stiffness, respectively. The time derivatives of the displacement are denoted (\dot{y}) for the velocity and (\ddot{y}) for the acceleration. The response of all structural dynamic systems involves a certain degree of damping and if a continuing state of vibration is studied then damping may be a very important factor to consider. However, the effects of damping are rarely considered in the analysis of structures subjected to blast loads because damping has very little effect on the maximum deflection, which usually is the only response of interest (Baker *et al.*, 1983). The reason for this is that structural damping is

much lower than for other systems where critical damping does need to be considered. In addition, the energy absorbed due to plastic deformations of the element is much greater than that absorbed by structural damping. Plastic response may be modeled with the use of SDOF analysis as shown in this section. Thus, the equation of motion can be reduced to:

$$m\ddot{y} + ky = P(t) \quad (4)$$

The natural circular frequency is given by:

$$w = \sqrt{\frac{k}{m}} \quad (5)$$

With the natural period of the system given by:

$$T_n = 2\pi \sqrt{\frac{m}{k}} = \frac{2\pi}{w} \quad (6)$$

A closed solution of the equation of motion was possible only when the loading and the resistance functions can be expressed in relatively simple mathematical terms. In other cases a numerical analysis can be used.

a. Modeling of retrofitted masonry walls as equivalent SDOF system

In the analysis of blast loaded structures it was convenient to model the real structure as an equivalent SDOF system. The equivalent system was determined on the principle of kinematic equivalency; i.e., the acceleration, velocity, and displacement were the same as that for a significant point on the actual structure, such as at center-point of a panel. This required the assumption of a deformed shape of the real structure. In order to define this mass-spring system in Figure 13 the equivalent mass m , force P and stiffness k , respectively, needed to be evaluated and these properties were derived from energy relationships. Thus, the external work, the strain

energy and the kinetic energy of the simplified system equaled the corresponding quantities of the real structure (Biggs, 1964). It was then convenient to introduce transformation factors to convert the properties of the real structure into the equivalent system. The derivations of the transformation factors K_M and K_L were reported and listed for beams and slabs with different end conditions and deformed shapes by Biggs (1964). Here, the chosen transformation factors were taken from Biggs (1964). Thus, in the elastic region the mass factor was $K_M=0.5$ and the load factor was $K_L=0.64$; whereas, in the plastic region, the mass factor was $K_M=0.33$ and the load factor was $K_L=0.5$.

The equation of motion of equivalent SDOF model took the form of:

$$m_e \ddot{y} + k_e y = P_e(t) \quad (7)$$

For this study, a Numerical Method using Finite Element simulation was used to determine the resistance function or load-deflection curves for masonry panels. Push-Over Static Analysis with Fiber Model Technique was performed using SAP2000 finite element software to get the load deflection curve for three retrofitted CMU panels. Then an in house MATLAB code was used to get the equivalent bilinear curve using Energy-Based Method. The results were shown in Figure 14.

The load-time function played an important role in the dynamic response of structural elements. An air blast load on a structure was essentially a single pulse, usually idealized by a simple geometric shape that gave a good resemblance of the actual blast wave. The type of load considered here was the triangular load with zero rise time. Thus, the system was subjected to an initial suddenly applied load P_o , which then decreased linearly to zero at time t_d , see Figure 15.

A close form solution of the equation of motion was possible only when the loading and the resistance functions could be expressed in relatively simple mathematical terms. In other cases a

numerical analysis could be used to solve the equation of motion step-by-step starting at zero time. Here in house MATLAB code was used to solve the equation of motion using non-linear Newmark method.

b. Iso-damage (Pressure-Impulse) curves

The use of iso-damage curves gave a good graphical representation of the capacity of panels when exposed to blast loads. Iso-damage curves were set up using wide range of applied triangular pressure loads with different blast durations. Then, the air blast test results were inserted into the calculated iso-damage curves as shown in Figure 16. The iso-damage curves for all three materials were superimposed over each other to compare the most efficient material to use, Figure 17.

7. CONCLUSIONS

The viability of using Nano Particle Reinforced Composites to protect masonry structures against blast loading was investigated experimentally, numerically, and analytically in this paper. Quarter scale model CMU walls made of scaled down brick units were retrofitted with NPREM material and subjected to a pre-adjusted airblast pressure and impulse. Three combinations of NPREM were used, which include using polyurea alone, polyurea reinforced with exfoliated graphine nano platelets (XGnP), and polyurea reinforced with Polyhedral Oligomeric Silsesquioxane[®] (POSS). A computationally-efficient model was built using an explicit hydrocode called ANSYS AUTODYN to replicate with reasonable accuracy the wall failure mechanisms, midpoint deflection, and debris velocity of retrofitted CMU walls subjected to blast loads. Then SDOF model was built and then used to establish iso-damage (pressure-impulse) curves. These curves were used as a tool to evaluate the behavior of retrofitted masonry walls under blast loads. Results from blast experiments showed an increase in ultimate flexural

resistance achieved by both unreinforced and nano-reinforced polyurea retrofit systems applied to URM wall. Whereas, nano reinforcing polyurea with POSS nano material improved the performance of the elastomeric retrofit for blast loading, XGnP addition showed very little improvement. Further investigations are underway to understand the physics behind these behaviors. Finite element results were compared to high-speed video images, midpoint deflection, and debris velocities obtained from experimental data. This study found that the model had the ability to replicate experimental results with good agreement, generally matching failure shape, location of break lines, and midpoint deflection at failure. However, it was also found that, without knowledge of actual material properties of the specific wall to be modeled, computational results were not reliable predictors of wall behavior.

8. ACKNOWLEDGEMENT

The preparation of the XGnP reinforced polyurea and the consultation on material properties provided by Dr. Larry Drzal of Michigan State University and XG Sciences is deeply appreciated. The preparation of POSS reinforced polyurea and consultation provided by Drs. Joe Lichtenhan and Bruce Fu of Hybrid Plastics is also gratefully acknowledged.

This work was partially supported by the funding received under a subcontract from the Department of Homeland Security-Sponsored Southeast Region Research Initiative (SERRI) at the Department of Energy's Oak Ridge National Laboratory, USA.

9. REFERENCES

- [1] Myers, J. J., Belarbi, A., and El-Domiaty, K. A. (2004). "Blast resistance of FRP retrofitted un-reinforced masonry (URM) walls with and without arching action", *TMS Journal*, 9-26.
- [2] Davidson, J. S., Porter, J. R., Dinan, R. J., Hammons, M. I., and Connell, J. D. (2004). "Explosive testing of polymer retrofit masonry walls", *ASCE Journal of Performance of Constructed Facilities*, 100-106
- [3] Johnson, C. F., Slawson, T. R., Cummins, T. R., and Davis, J. L. (2005). "Concrete masonry unit walls retrofitted with elastomeric systems for blast loads", *Proceedings for the Army Science Conference (24th)*, Orlando, Florida.
- [4] Davidson, J. S., Fisher, J. W., Hammons, M. I., Porter, J. R., and Dinan, R. J. (2005). "Failure mechanisms of polymer-reinforced concrete masonry walls subjected to blast", *ASCE Journal of Structural Engineering*, 1194-1206.
- [5] Muszynski, L. C., and Purcell, M. R. (2003). "Use of composite reinforcement to strengthen concrete and air-entrained concrete masonry walls against air blast", *ASCE Journal of composites for Construction*, 98-108.
- [6] Ghobarah, A., and El Mandooh, G. K. (2004). "Out-of-plane strengthening of unreinforced masonry walls with openings", *ASCE Journal of Composites for Construction*, 298-305.
- [7] Eamon, C. D., Baylot, J. T., and O'Daniel, J. L. (2004). "Modeling concrete masonry walls subjected to explosive loads", *ASCE Journal of Engineering Mechanics*, 1098-1106.

- [8] Naito, C. J., and Wheaton, K. P. (2006). "Blast assessment of load-bearing reinforced concrete shear walls", *Practice Periodical on Structural Design and Construction*, 11(2), 112–121.
- [9] Baker, W. E., Cox, P. A., Westine, P. S., Kulesz, J. J., Strehlow, R. A. (1983). "Explosion Hazards and Evaluation", *Elsevier*, New York.
- [10] Biggs, J. M. (1964). "Introduction to Structural Dynamics", *McGraw-Hill*, New York.

LIST OF FIGURES

- Figure 1: Material Testing and Simulation (MTS) machine
- Figure 2: Typical stress-strain relation for retrofitted materials under tensile loading
- Figure 3: (a) Masonry wall dimensions (b) Concrete masonry unit brick (all dimensions in mm) (c) comparison between full scale and scaled down dimensions of masonry unit
- Figure 4: Blast simulator, Vicksburg, MS
- Figure 5: Spray-on retrofitted material
- Figure 6: Locations of pressure sensors (P1-P6) and typical peak pressure values
- Figure 7: Typical pressure-time history and associated impulse time history obtained for Wall 3 using pressure Sensor.
- Figure 8: Wall #1 (a) back view before the blast event (b) back view after the blast event (c) front view after the blast event
- Figure 9: Wall #2 (a) front view before the blast event (b) front view after the blast event (c) back view after the blast event
- Figure 10: Wall #3 (a) back view after the blast event (b) front view after the blast event
- Figure 11: (a) Wall geometry (b) F.E. mesh
- Figure 12: Single degree of freedom system
- Figure 13: Equivalent SDOF system
- Figure 14: Resistance function (Load deflection) curves for CMU panels retrofitted using (a) polyurea alone (b) Polyurea with POSS (c) polyurea with xGnP
- Figure 15: Triangular load approximation airblast
- Figure 16: Iso-damage curves (Pressure-Impulse) for masonry panels retrofitted with (a) Polyurea alone (b) Polyurea with xGnP (c) Polyurea with POSS
- Figure 17: Iso-damage curves for polyurea, POSS reinforced polyurea, and xGnP reinforced polyurea (ductility =1)

LIST OF TABLES

- Table 1: Retrofitted materials properties
- Table 2: Test matrix of retrofitted schemes
- Table 3: Retrofitted layer thicknesses
- Table 4: Average values of reflected pressure and impulse for each wall
- Table 5: Material models
- Table 6: Deformation and failure shapes obtained numerically and experimentally for the case of CMU wall retrofitted with polyurea (wall #1)
- Table 7: Failure shapes obtained numerically and experimentally for the case of CMU wall retrofitted with xGnP reinforced polyurea (wall #2)
- Table 8: Failure shapes obtained numerically and experimentally for the case of CMU wall retrofitted with POSS reinforced polyurea (wall #3)
- Table 9: Midpoint deflection and debris velocity

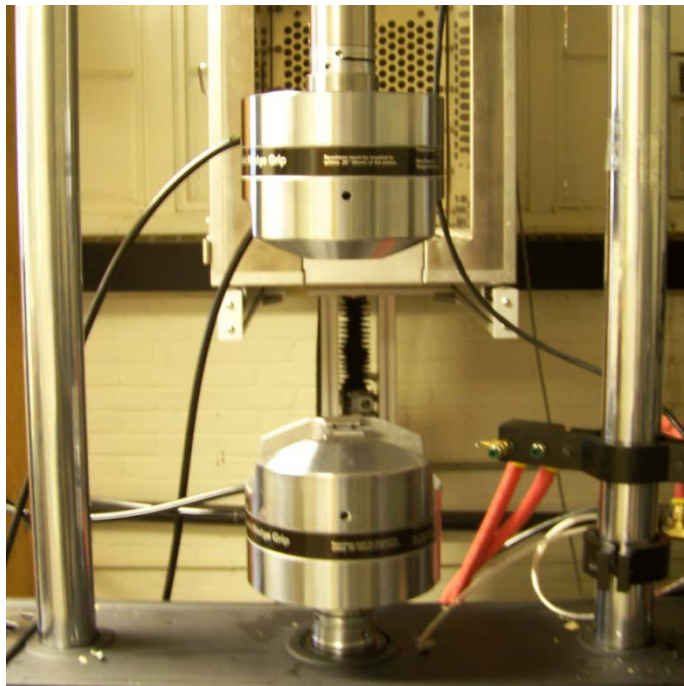


Figure 18: Material Testing and Simulation (MTS) machine

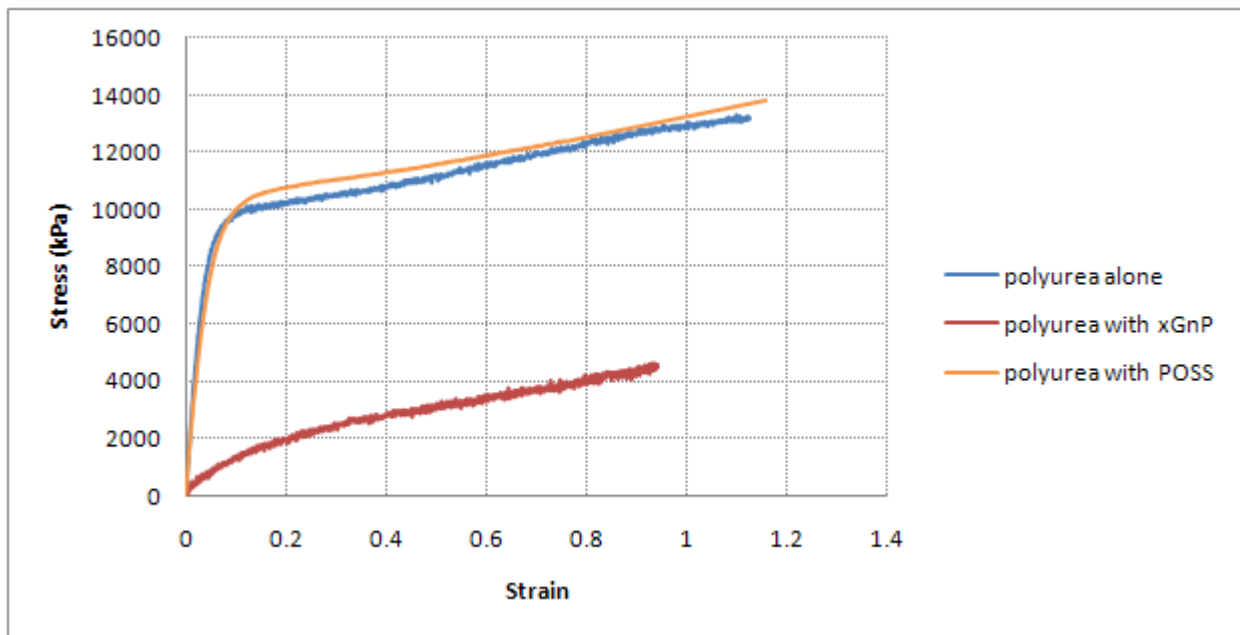


Figure 19: Typical stress-strain relation for retrofitted materials under tensile loading

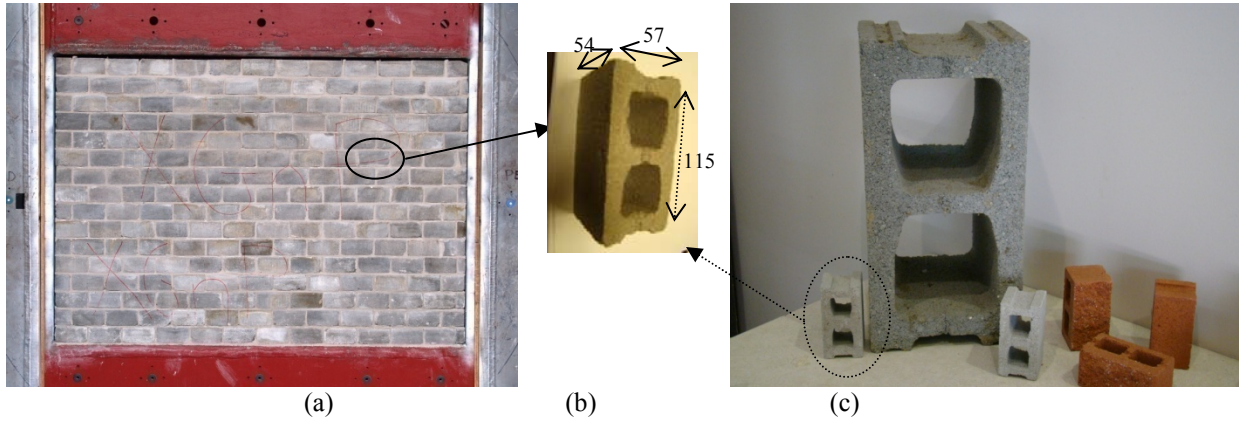


Figure 20: (a) Masonry wall dimensions (b) Concrete masonry unit brick (all dimensions in mm) (c) comparison between full scale and scaled down dimensions of masonry unit



Figure 21: Blast simulator, Vicksburg, MS



Figure 22: Spray-on retrofitted material

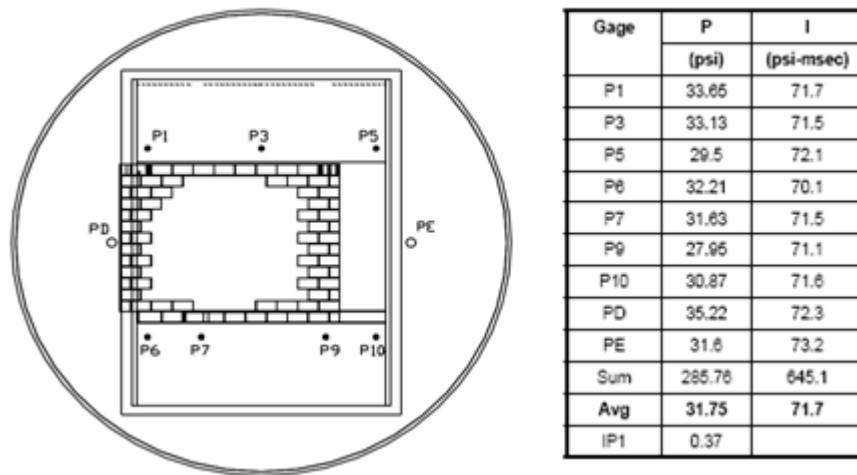


Figure 23: Locations of pressure sensors (P1-P6) and typical peak pressure values

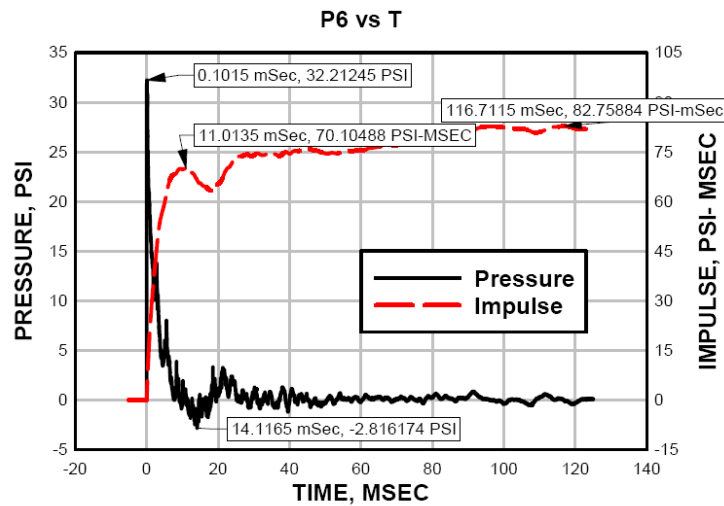


Figure 24: Typical pressure-time history and associated impulse time history obtained for Wall 3 using pressure Sensor.

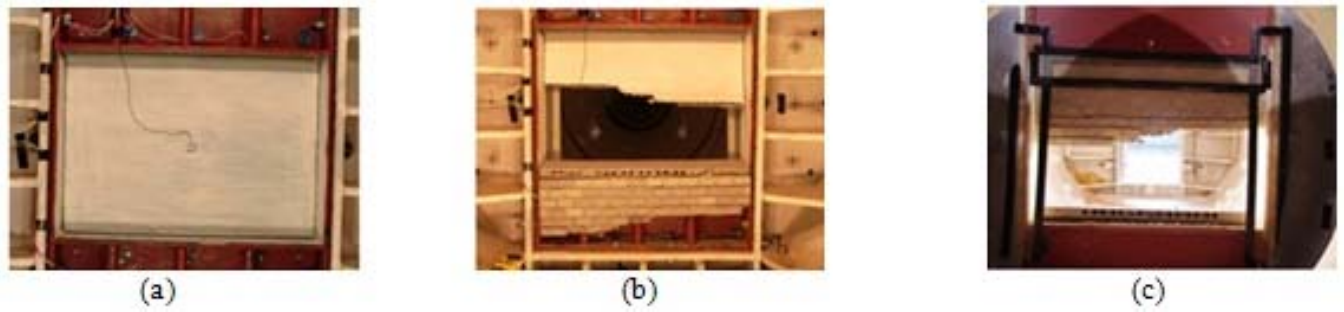


Figure 25: Wall #1 (a) back view before the blast event (b) back view after the blast event (c) front view after the blast event



Figure 26: Wall #2 (a) front view before the blast event (b) front view after the blast event (c) back view after the blast event



Figure 27: Wall #3 (a) back view after the blast event (b) front view after the blast event

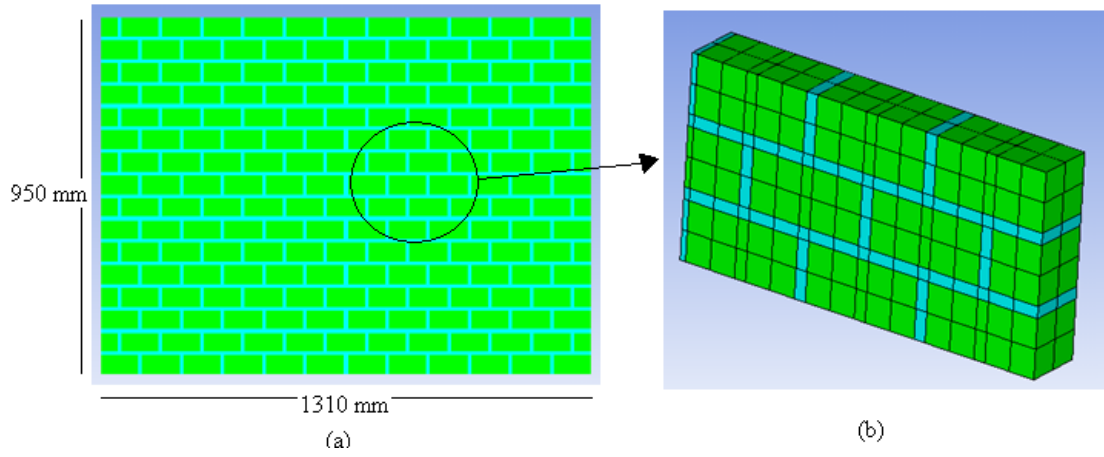


Figure 28: (a) Wall geometry (b) F.E. mesh

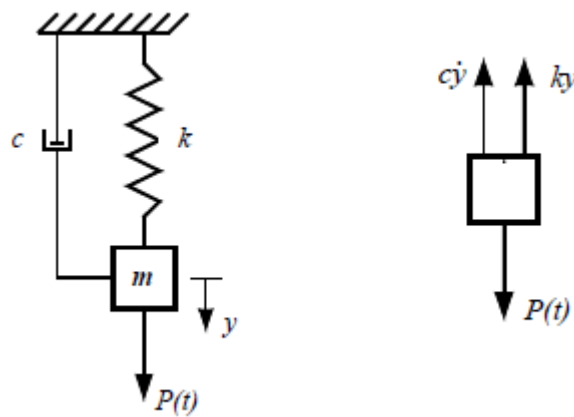


Figure 29: Single degree of freedom system

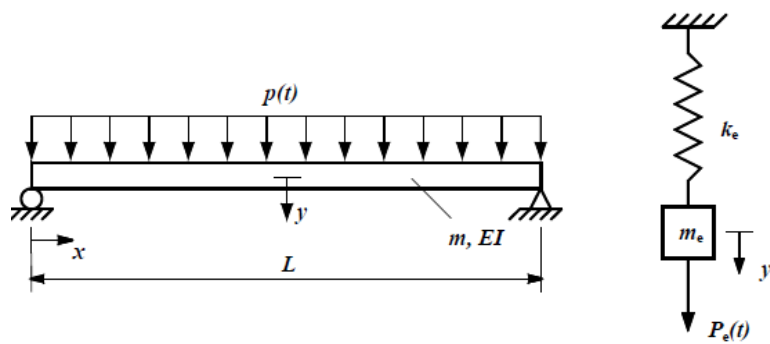
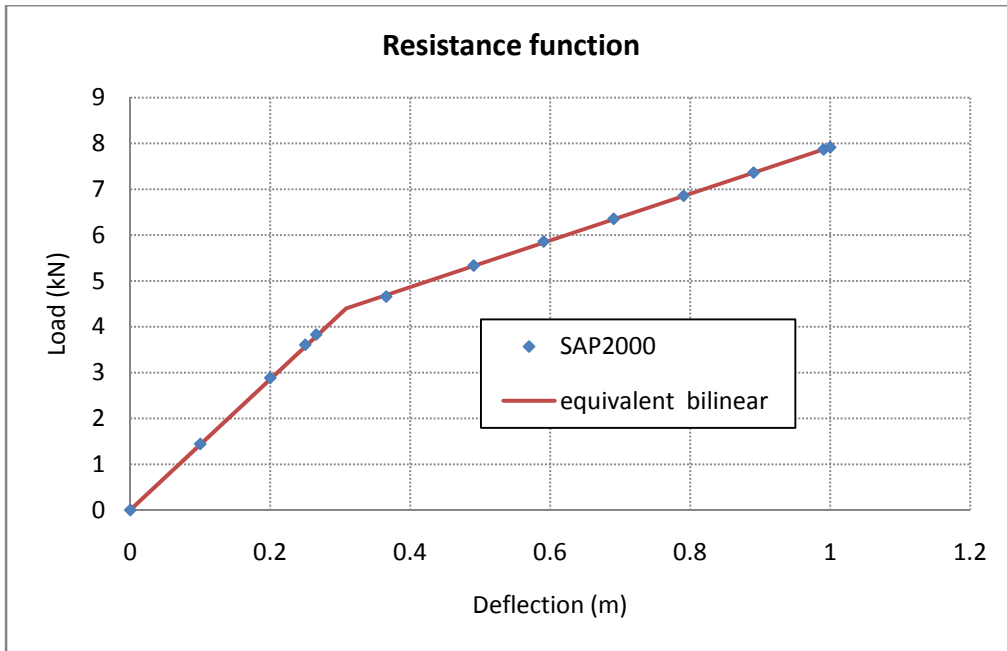
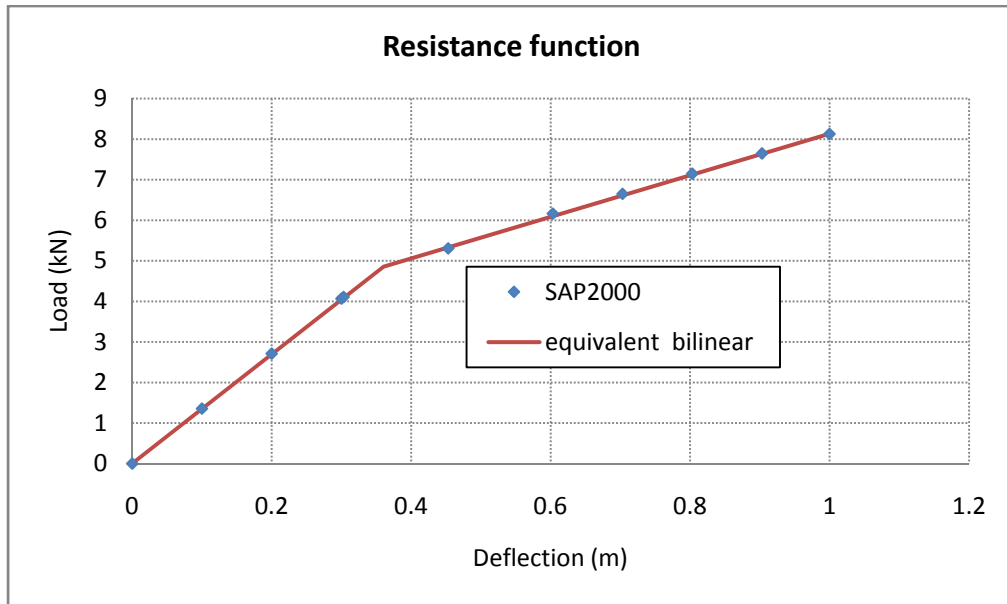


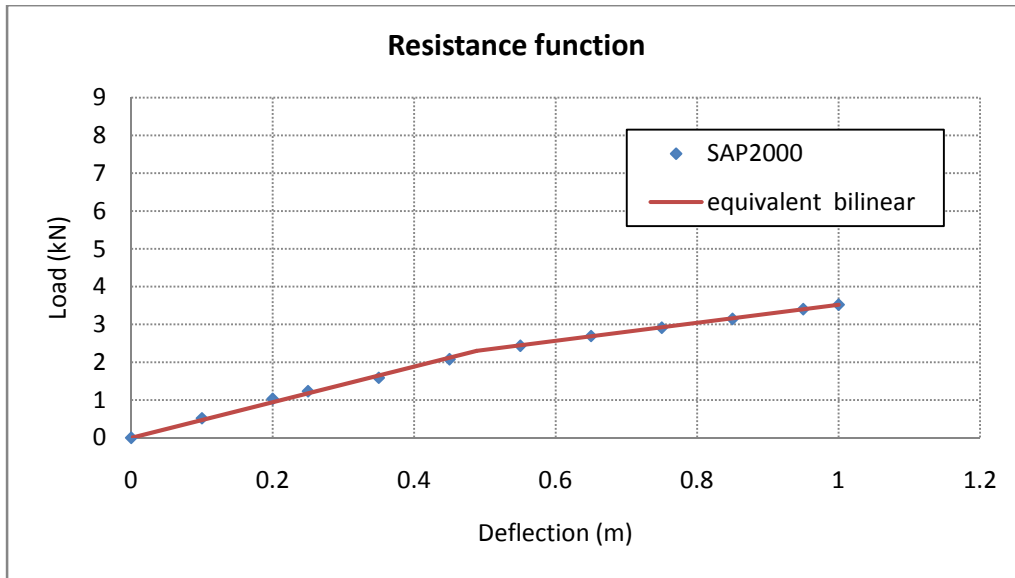
Figure 30: Equivalent SDOF system



(a)



(b)



(c)

Figure 31: Resistance function (Load deflection) curves for CMU panels retrofitted using (a) polyurea alone (b) Polyurea with POSS (c) polyurea with xGnP

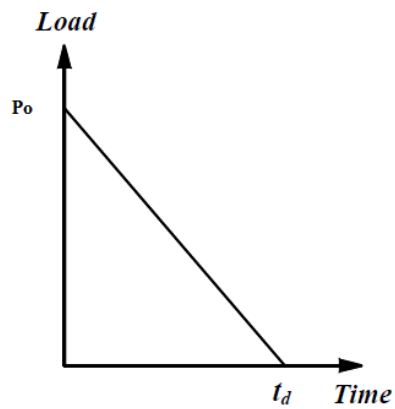
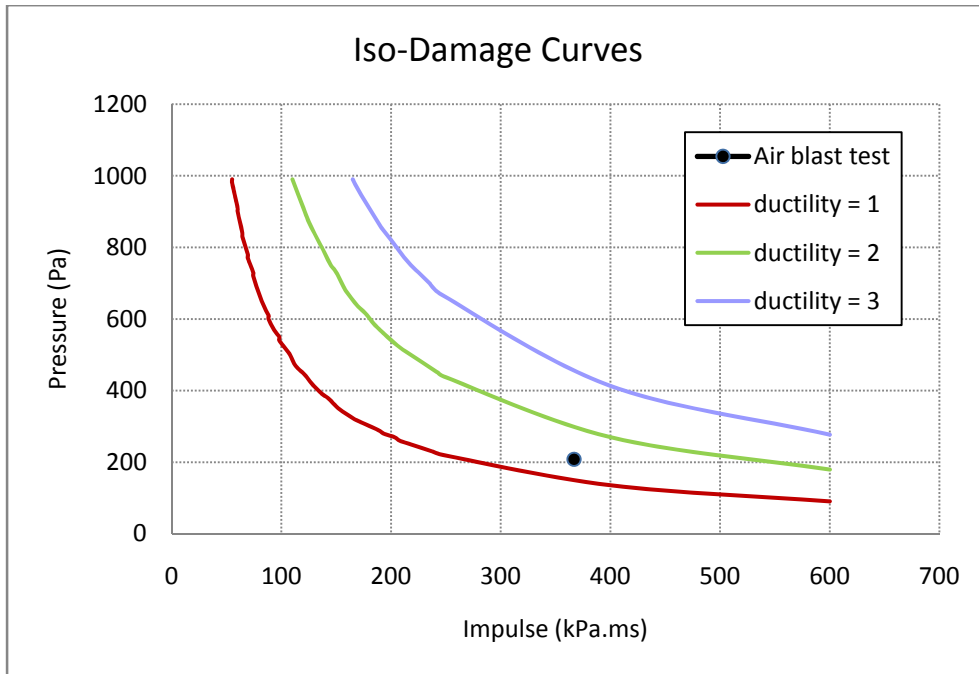
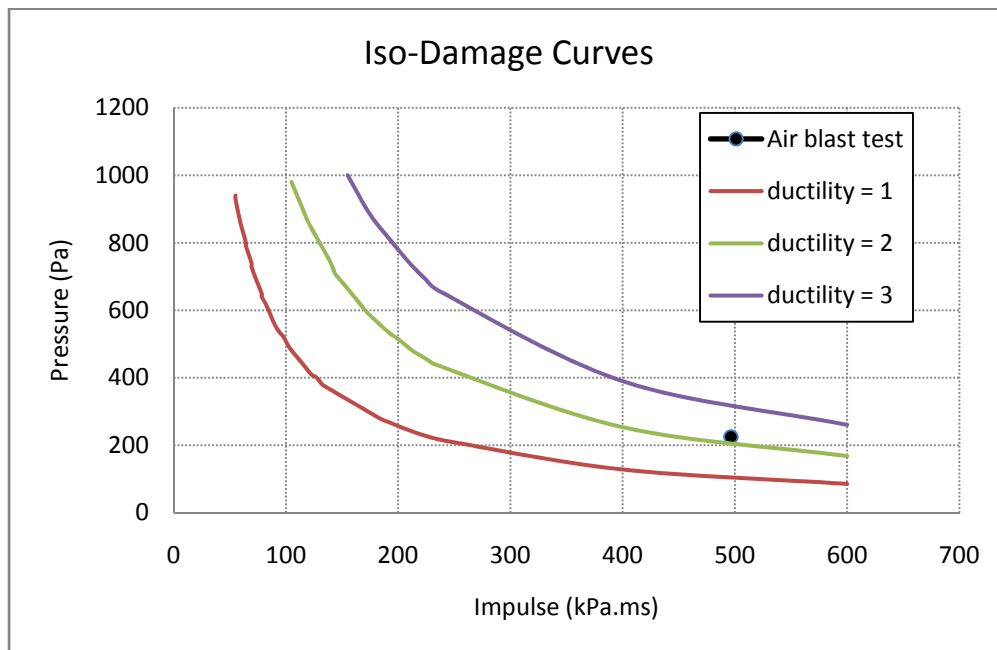


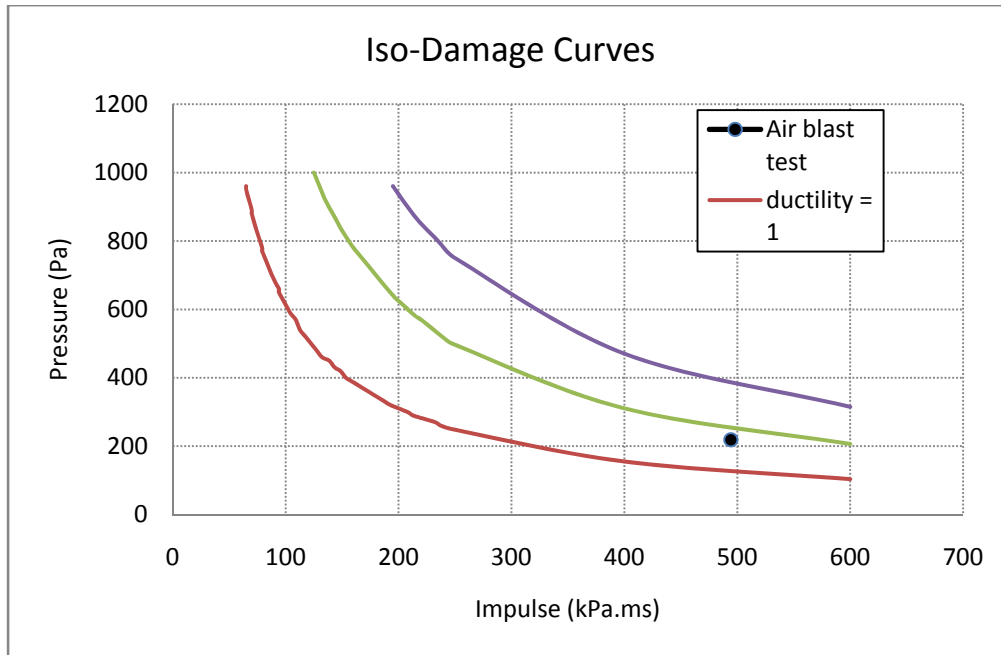
Figure 32: Triangular load approximation airblast



(a)



(b)



(c)
 Figure 33: Iso-damage curves (Pressure-Impulse) for masonry panels retrofitted with (a) Polyurea alone (b) Polyurea with xGnP (c) Polyurea with POSS

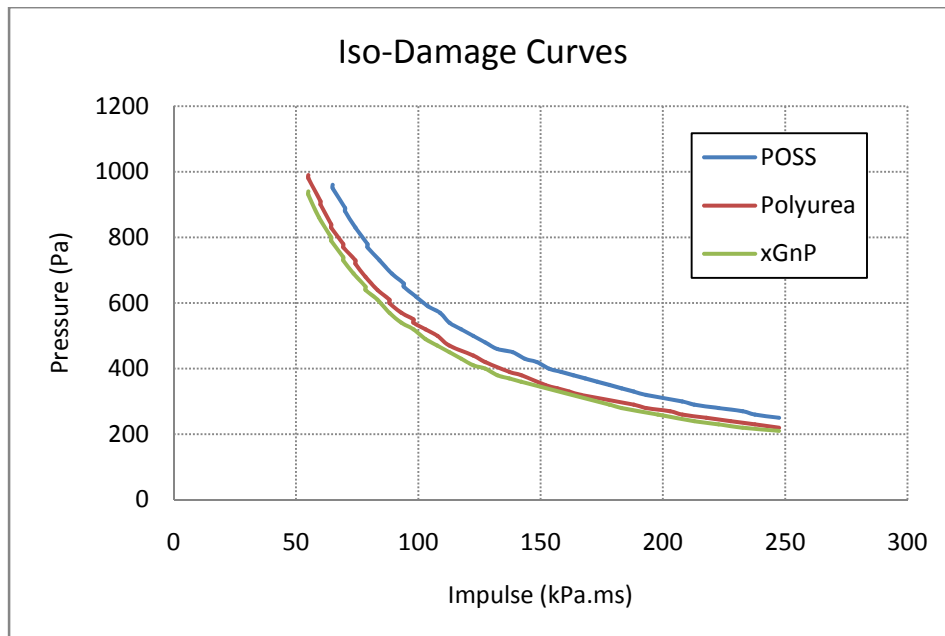


Figure 34: Iso-damage curves for polyurea, POSS reinforced polyurea, and xGnP reinforced polyurea (ductility = 1)

Table 10: Retrofitted materials properties

Material	Modulus of Elasticity (MPa/ psi)	Ultimate Strength (MPa/ psi)	Strain at Rupture (%)
Polyurea	229.46/ 33280.00	13.29/1927.49	113
Polyurea with xGnP	12.06/1749.00	4.59/666.38	94
Polyurea with POSS	210.56/30539.25	13.81/2003.17	116

Table 11: Test matrix of retrofitted schemes

Wall Number	Retrofit Material
Wall #1	polyurea alone
Wall #2	polyurea reinforced with xGnP
Wall #3	polyurea reinforced with POSS

Table 12: Retrofitted layer thicknesses

Wall Number	Retrofit Layer Thickness, mm
Wall #1	1.5
Wall #2	1.5
Wall #3	1.8

Table 13: Average values of reflected pressure and impulse for each wall

Wall Number	Pressure kPa, (psi)	Impulse (kPa.ms) (psi.ms)
Wall #1	208.22 (30.20)	366.80 (53.20)
Wall #2	224.91 (32.62)	496.42 (72.00)
Wall #3	218.91 (31.75)	494.35 (71.70)

Table 14: Material models

Material	EOS	Strength Model	Failure Model
Masonry	Porous	Drucker-Prager	Hydrodynamic tensile failure (P_{min})
Mortar	Compaction	Mo Granular	Hydrodynamic tensile failure (P_{min})
Polyurea	Linear	Johnson-Cook	Principal Strain
Poyurea with POSS	Linear	Johnson-Cook	Plastic strain
Poyurea with xGnP	Linear	Johnson-Cook	Principal Strain

Table 15: Deformation and failure shapes obtained numerically and experimentally for the case of CMU wall retrofitted with polyurea (wall #1)

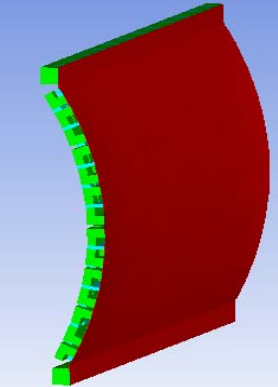
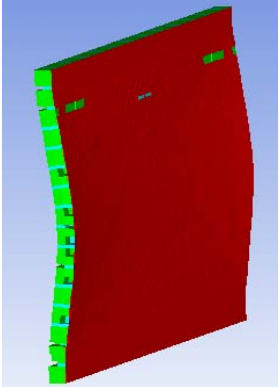


Beginning of the Failure	Final Stage	
		<p>Numerical Results obtained using AUTODYN hydrodynamic code</p>
		<p>Experimental results obtained using BLS</p>

Table 16: Failure shapes obtained numerically and experimentally for the case of CMU wall retrofitted with xGnP reinforced polyurea (wall #2)

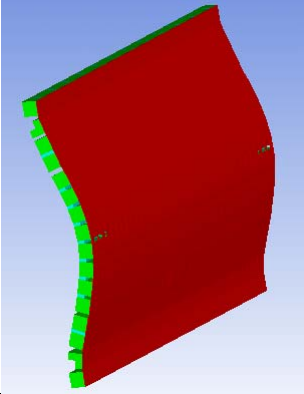
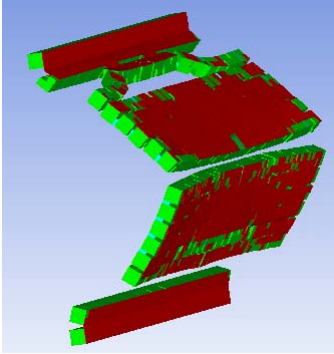


Beginning of the Failure	Final Stage	
		<p>Numerical Results obtained using AUTODYN hydrodynamic code</p>
		<p>Experimental results obtained using BLS</p>

Table 17: Failure shapes obtained numerically and experimentally for the case of CMU wall retrofitted with POSS reinforced polyurea (wall #3)

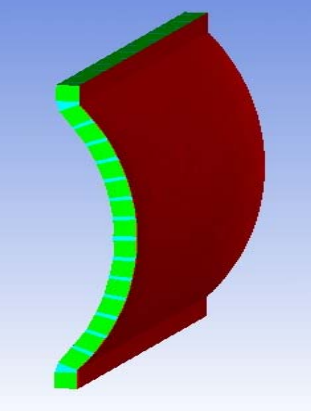
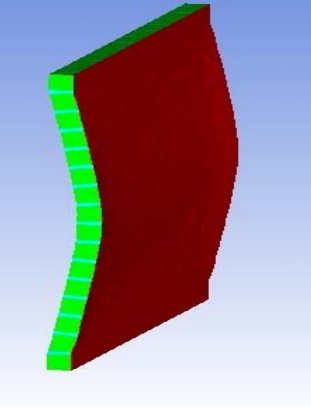


Maximum deflection	final stage	
		<p>Numerical Results obtained using AUTODYN hydrodynamic code</p>
		<p>Experimental results obtained using BLS</p>

Table 18: Midpoint deflection and debris velocity

Wall Number	Midpoint deflection at failure mm		maximum debris velocity m/s	
	Experiments	Finite element	Experiments	Finite element
Wall #1	91.4	102.61	3.86	4.44
Wall #2	76.4	113	7.47	6.14
Wall #3	95.65	112	N.A	N.A